

# Quantitative assessment of mandibular cortical erosion on dental panoramic radiographs for screening osteoporosis

Chisako Muramatsu<sup>1</sup> · Kazuki Horiba<sup>1</sup> · Tatsuro Hayashi<sup>2</sup> · Tatsumasa Fukui<sup>3</sup> · Takeshi Hara<sup>1</sup> · Akitoshi Katsumata<sup>3</sup> · Hiroshi Fujita<sup>1</sup>

Received: 25 January 2016 / Accepted: 31 May 2016 / Published online: 11 June 2016  
© CARS 2016

## Abstract

**Purpose** Studies reported that the mandibular cortical width (MCW) measured on dental panoramic radiographs (DPRs) was significantly correlated with bone mineral density. However, MCW is not a perfect index by itself, and studies suggest the added utility of mandibular cortical index (MCI). In this study, we propose a method for computerized estimation of mandibular cortical degree (MCD), a new continuous measure of MCI, for osteoporotic risk assessment.

**Methods** The mandibular contour was automatically segmented using an active contour model. The regions of interest near mental foramen were extracted for MCW and MCD determination. The MCW was measured on the basis of residue-line detection results and pixel profiles. Image features including texture features based on gray-level co-occurrence matrices were determined. The MCD were estimated using support vector regression (SVR). The SVR was trained using previously collected 99 DPRs, including 26 osteoporotic cases, by a computed radiography system. The proposed scheme was tested using 99 DPRs obtained by a photon-counting system with data of bone mineral density at distal forearm. The number of osteoporotic, osteopenic, and control cases were 12, 18, and 69 cases, respectively. The subjective MCD by a dental radiologist was employed for training and evaluation.

**Results** The correlation coefficients with the subjective MCD were  $-0.549$  for MCW alone,  $0.609$  for the MCD by the features without MCW, and  $0.617$  for the MCD by the features and MCW. The correlation coefficients with the BMD were  $0.619$ ,  $-0.608$ , and  $-0.670$ , respectively. The areas under the receiver operating characteristic curves for detecting osteoporotic cases were  $0.830$ ,  $0.884$ , and  $0.901$ , respectively, whereas those for detecting high-risk cases were  $0.835$ ,  $0.833$ , and  $0.880$ , respectively.

**Conclusions** In conclusion, our scheme may have a potential to identify asymptomatic osteoporotic and osteopenic patients through dental examinations.

**Keywords** Dental panoramic radiographs · Mandibular cortex erosion · Mandibular cortical width · Osteoporosis · Textural features

## Introduction

Osteoporosis is characterized by low bone mass and structural deterioration of the bone tissue and is regarded as a major public health problem, especially in the aging world population. It is estimated that 200 million or more women are affected by the disease worldwide [1]. This asymptomatic disease can lead unnoticeably to bone weakness and elevate susceptibility to fractures of the hip, vertebra, and forearm. There were an estimated nine million osteoporotic fractures worldwide in 2000, which could be related to a cause of death and certainly accounted for the disability of patients [2,3]. Early diagnosis and treatment can contribute to a reduction of the number of severe fractures and medical costs.

Studies have reported an association between the mandibular cortical width (MCW) on dental panoramic radiographs (DPRs) and bone mineral density (BMD), suggesting the pos-

✉ Chisako Muramatsu  
chisa@fjt.info.gifu-u.ac.jp

<sup>1</sup> Department of Intelligent Image Information, Graduate School of Medicine, Gifu University, 1-1 Yanagido, Gifu, Gifu 501-1194, Japan  
<sup>2</sup> Media Co., Ltd, 3-26-6 Hongo, Bunkyo-ku, Tokyo 113-0033, Japan  
<sup>3</sup> Department of Oral Radiology, Asahi University School of Dentistry, 1851 Hozumi, Mizuho, Gifu 501-0296, Japan

sible screening of asymptomatic osteoporotic patients with DPRs [4–6]. DPRs are used frequently throughout the world for examining dental conditions. More than ten million DPRs are obtained each year in dental clinics in the USA and Japan [7, 8]. However, dental practitioners are generally not reviewing the extra-dental regions. Even if they are, it is extremely rare that the MCW is quantitatively evaluated during a dental practice.

To enable quantitative assessment and assist in the early detection of osteoporosis, several research groups have suggested automated or semiautomated methods for the measurement of the MCW [9–12]. Arifin et al. [9] proposed a semiautomated method, where regions of interests (ROIs) below mental foramen identified by an examiner are processed by a high-pass filter to identify the cortical margins. In that study, inner and outer cortical margins were determined by gradient analysis with manual assistance. In their recent study [10], after manual extraction of the ROIs, the cortical margin was automatically segmented using dynamic programming, and cases with low BMD and normal BMD were classified on the basis of MCW histogram analysis using a support vector machine. An evaluation with 60 training and 40 test cases demonstrated the potential usefulness of their method with sensitivities of 96% and specificities of 86 and 84% for low BMD at the lumbar spine and femoral neck, respectively. Allen et al. [11] and Roberts et al. [12] proposed a computerized method to determine the lower and upper cortical borders using active shape models and subsequently active appearance models without and with manual annotation points. Although they encountered some failure cases in the fully automatic mode, the MCW was useful in detecting cases with low BMD at the femoral neck with the sensitivity of 80% and the specificity of approximately 77% in 663 cases.

We have previously proposed a fully automatic method for the measurement of the MCW based on a mandibular contour model fitting and profile analysis [13, 14]. Using 100 cases, the high sensitivity and specificity of 80.8 and 94.6%, respectively, for identifying osteoporotic patients were obtained, indicating the potential benefit of our system in a role of supplemental screening. The system was implemented in a teleradiology service and is in a trial operation. However, the sensitivity is not a perfect with the MCW measurement alone, even with the manual measurement.

On the other hand, Taguchi et al. [15] suggested that cortical erosion characterized by endosteal residue or porosity could be a sign indicative of osteoporotic risk; its condition can be classified into the three mandibular cortical index (MCI) grades suggested by Klemetti et al. [16] In fact, several groups have studied fractal analysis and morphologic analysis on dental radiographs for evaluating the structural change in alveolar and trabecular bones and detecting women with low BMD [17–21]. Some of these studies found the useful-

ness of the analysis [17, 20], whereas others found no strong association [18, 19, 21]. One of the reasons for limited usefulness might be that the fractal dimension by itself cannot fully describe coarseness of cortical bone.

More recently, Nakamoto et al. [22, 23] proposed an automated method to determine cortical erosion on DPRs for screening osteoporosis. In their studies, the ROIs around the cortical bone were extracted, and the bright regions were detected by morphological skeletonization. Based on the detected line segments, images were classified into normal-BMD and low-BMD groups. Roberts et al. [24] investigated the texture features to capture the cortical holes and residues for improving the computerized diagnosis of osteoporosis on DPRs. They determined Haralick texture features and used a random forest classifier to predict the probability of osteoporosis. They demonstrated that the cortical texture combined with the cortical width could be a strong biomarker for osteoporosis at the femoral neck. Kavitha et al. [25] performed a similar study and concluded that the combination of texture features and the MCW can be a superior indicator of osteoporosis. A conclusion of Robert et al. [24] was that texture classifiers perform more effectively than the MCI assigned by experts, probably owing to its subjective nature and coarse categorization.

In this study, we investigate image features to characterize the cortical condition and automatically quantify the degree of mandibular cortical erosion. In our preliminary investigation [26], we attempted to classify cases into three MCI groups. Although the result with a leave-one-out cross-validation confirmed a potential utility of our method, the classification of Class II cases was difficult partly owing to the ambiguity of class definitions. Our aim is to not only detect patients with osteoporotic risk but also provide quantitative data that can be useful to dentists in recommending further examinations for patients. For improving the classification and quantification, we investigate the use of a continuous rate, which we call the mandibular cortical erosion degree (MCD), rather than discrete classes, to potentially overcome coarse categorization of MCI and to enhance the system training.

## Materials and methods

### DPR datasets

The first dataset was collected in our previous study and consists of 99 DPRs [13]; one case was excluded because of its atypical cortical morphology. The dataset includes 82 cases obtained during routine dental examinations where 26 cases have been diagnosed with osteoporosis by clinical evaluation with dual-energy X-ray absorptiometry (DXA), and 17 cases were normal volunteers. Thirty-five subjects were male and 59 were female with mean ages of 54 and 57, respectively.

The age and/or gender information was missing in five cases. The images were obtained with Veraview Epos (J. Morita MFG. Corp., Kyoto, Japan) and CR 75.0 (Agfa, Mortsels, Belgium) at Asahi University Hospital, Gifu, Japan. They were in Digital Imaging and Communications in Medicine (DICOM) format with  $1420 \times 2920$  pixels, 0.1-mm resolution, and 12-bit grayscale.

The second dataset was obtained with QRmaster-PTM (Telesystems Co., Ltd., Osaka, Japan) at Asahi University Hospital for evaluation of periodontal diseases. It includes 99 patients who have undergone DXA measurements of the forearm with a simple equipment for research purposes. All patients do not have the history of osteoporotic diagnosis or known fractures. According to the World Health Organization (WHO) criterion, patients with a  $T$ -score, calculated by the measured BMD minus the young adult mean (YAM) of the BMD divided by the young adult standard deviation (SD) of the BMD, less than equal to  $-2.5$  are considered osteoporotic, whereas those with a  $T$ -score between  $-2.5$  and  $-1.0$  are considered osteopenic. Until 2012, the Japanese Society for Bone and Mineral Research and Japan Osteoporosis Society recommended the criteria of less than 70 and 80% of YAM of the BMD at the corresponding sites as osteoporosis and osteopenia, respectively. In 2012, they announced the new criteria in accordance with WHO; the cutoff values of 70% of YAM of the BMD and  $T$ -score of  $-2.5$  are comparable for lumbar spines and femoral neck. However, it is known that the young adult SD of distal radius is very small, causing a substantial difference between the two cutoff values. Therefore, it is recommended that the conventional 70 and 80% criteria would be used for

the BMD of the distal radius; we followed this recommendation to avoid overdiagnosis. Based on this criterion and assuming that they do not have non-traumatic fractures, the dataset consists of 12, 18, and 69 images of osteoporosis, osteopenia, and control cases, respectively. The history of other diseases related to the secondary osteoporosis, medication status, smoking history and alcohol consumption were not known. The mean ages of the 56 females and 43 males are 59 and 53, respectively. The images were saved in bitmap format with  $1573 \times 3024$  pixels, 0.1-mm resolution, and 8-bit grayscale. All procedures performed in studies involving human participants were in accordance with the ethical standards of the institutional research committee and with the 1964 Helsinki Declaration and its later amendments or comparable ethical standards. For this type of study, formal consent is not required.

The first dataset was used for training the system; the second dataset was used for evaluation. The images from the two datasets exhibit appreciable differences because of the different imaging systems, i.e., computed radiography versus photon-counting system. This enables the evaluation of the robustness of the proposed method. Figure 1 presents the phantom images and the corresponding histograms obtained with the two systems. They were imaged with routine automatic exposure settings. A notable difference in appearance can be observed. A dental radiologist graded the cortical erosion on a continuous scale from normal cortex (0.0) to severely eroded cortex (1.0) without other diagnostic information, and this subjective MCD was used for the system training and evaluation.

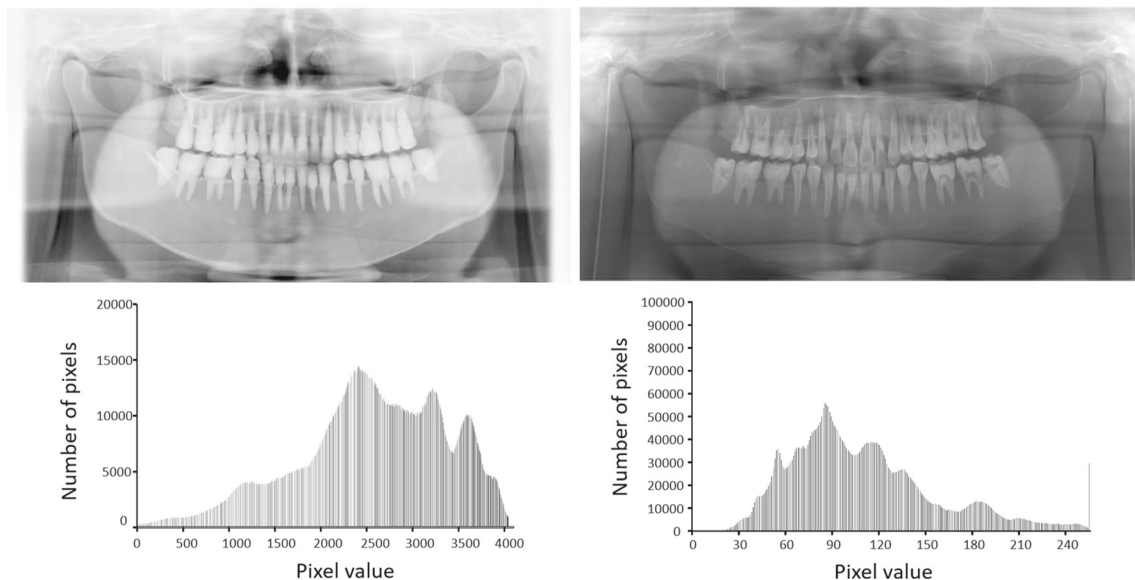


**Fig. 1** Dental panoramic radiographs of a phantom obtained by different imaging systems and the corresponding pixel value histograms: (left) by computed radiography system ( $1420 \times 2920$  pixels) and (right) by a photon-counting system ( $1573 \times 3024$  pixels)

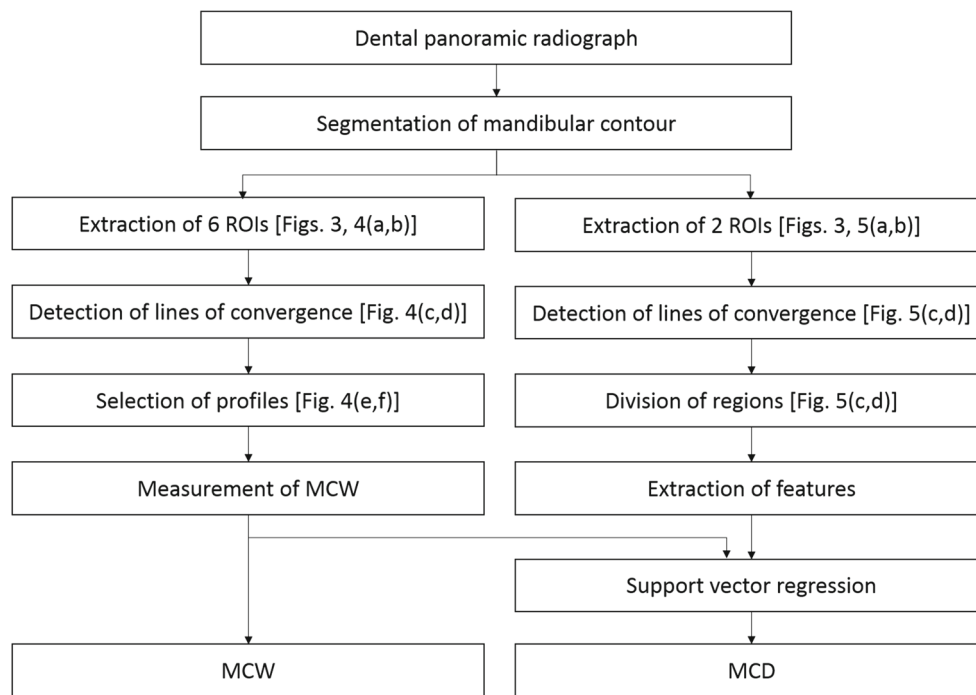


**Fig. 2** Flowchart of the proposed method. The *left side* describes the previous method for the MCW measurement and the *right side* is the new method added for MCD determination

## Method overview

The flow of the proposed method is illustrated in Fig. 2. Our computerized scheme begins with the extraction of regions of interests (ROIs) for the measurement of the MCW and determination of image features for cortical erosion. The lower border of the mandible was automatically segmented using Kirsch's Canny edge detector [27] and an active contour model. The details of the segmentation method are described elsewhere [13]. For measurement of the MCW, three ROIs of  $101 \times 100$  pixels were obtained for each of the right and left reference points. For feature analysis, one ROI of  $151 \times 100$  pixels around the reference point on each side was extracted.

When a cortex begins to erode, endosteal cortical residues appear as horizontal lines along the cortical margin. To detect these linear structures, the line convergence filter [28] was applied to all of the ROIs. Based on the detected ridges, the optimal position was selected for the measurement of the MCW. The filter outputs in the image analysis ROIs were used for determination of the image features characterizing the cortical texture. The ROI was divided into three regions, i.e., outer cortex region, marginal region, and inner trabecular region based on the profiles, and ridge related features were determined in the marginal region. Other features included Haralick's textural features based on the gray-level co-occurrence matrix (GLCM) [29]. Although the most common texture feature used for osteoporosis evaluation is fractal dimension, its descriptive power could be limited by itself.

To more thoroughly describe the texture, we employed and tested 13 features based on GLCM, which are commonly used to describe medical image texture. Upon removal of the features with low utility, principal component analysis (PCA) was applied, and the MCD was estimated by the support vector regression (SVR) [30].

## ROI extraction

MCW measurements are often made below the right and left mental foramen [31]. When a cortex is eroded, MCW measurement can be influenced by the cortical residues. In some cases, a shadow of hyoid bone is overlapped with the cortical bone, causing the mismeasurement of the MCW. To reduce the measurement errors, a set of 15 profiles, which is considered optimal for the measurement, was selected from the 101 candidate profiles in our previous study [14]. In this study, to further refine the measurement, these 101 profiles were obtained at six positions, corresponding to the three ROIs on each side, and four out of the six average measurements were employed by omitting the maximum and minimum MCWs to exclude possible outliers.

For each point of interest on the mandibular contour, a line was fitted using 21 pixels along the contour, and 100 pixel values were obtained along the line perpendicular to the fitted line as indicated in Fig. 3b. This process was repeated for the 101 or 151 points around the reference point for creating an ROI of  $101 \times 100$  (for the MCW measurement) or

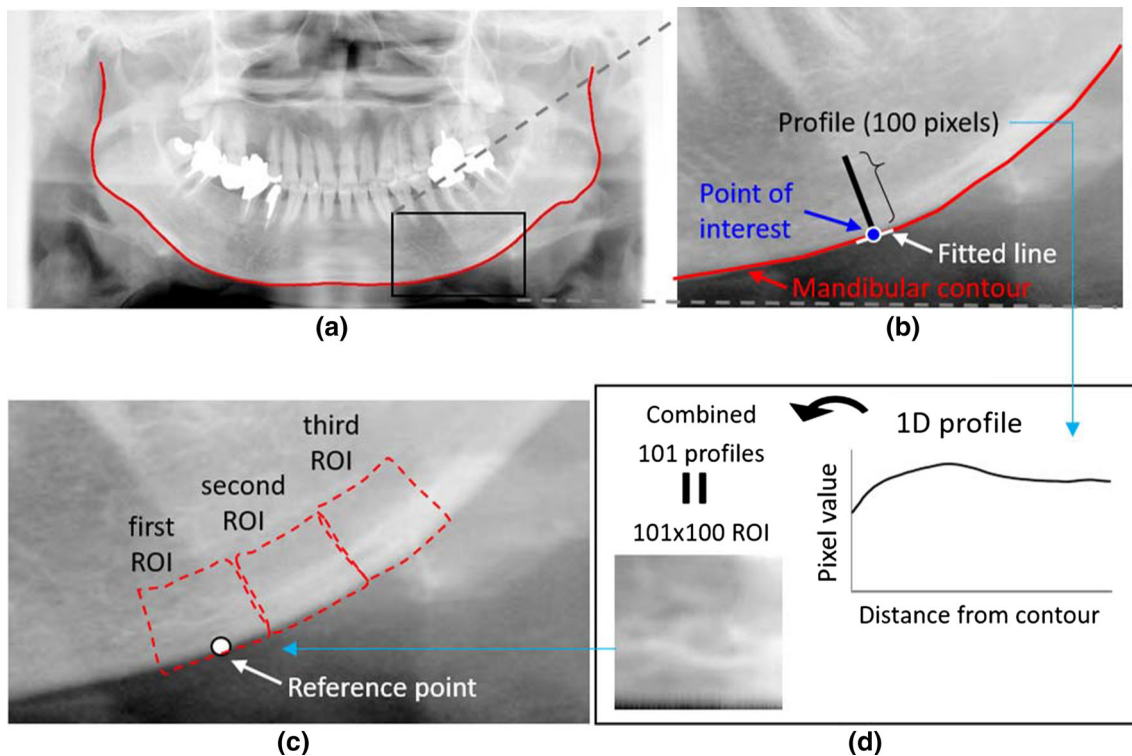


**Fig. 3** Obtaining a profile perpendicular to the line fitted to the mandibular contour for extraction of regions of interest (ROIs). **a** A dental panoramic radiograph with an automatic segmentation result of mandibular contour, **b** enlarged view of the cortex with a fitted line

(pseudo tangential line) and its perpendicular line (profile) for a point of interest, **c** an example of a profile and combined profiles for creating an ROI, and **d** positions of the second and third ROIs for the MCW measurement

151 × 100 (for feature analysis) pixels (Fig. 3c, d). Examples of the extracted ROIs for the MCW measurement and feature analysis are presented in Figs. 4a, b and 5a, b, respectively. The second and third ROIs for the MCW measurement were extracted in a similar manner by obtaining the profiles continuously in posterior to the first ROI as shown in Fig. 3c.

**Ridge detection and profile selection for MCW measurement [14]**

As an osteoporotic risk marker, we defined the MCW as the width of the dense cortex excluding the eroded margin area. Therefore, we searched for a border of dense cortex between the densest part, i.e., peak of the profile, and the cortical residues, if present. Therefore, horizontal ridges corresponding to the peak and possible residues were detected by the line convergence filter as illustrated in Fig. 4c, d [28]. When a ridge is present, the gradients on the both sides are perpendicularly converged to the ridge. The Prewitt filter was applied to determine the directions of the gradients. The normalized inner product was calculated by

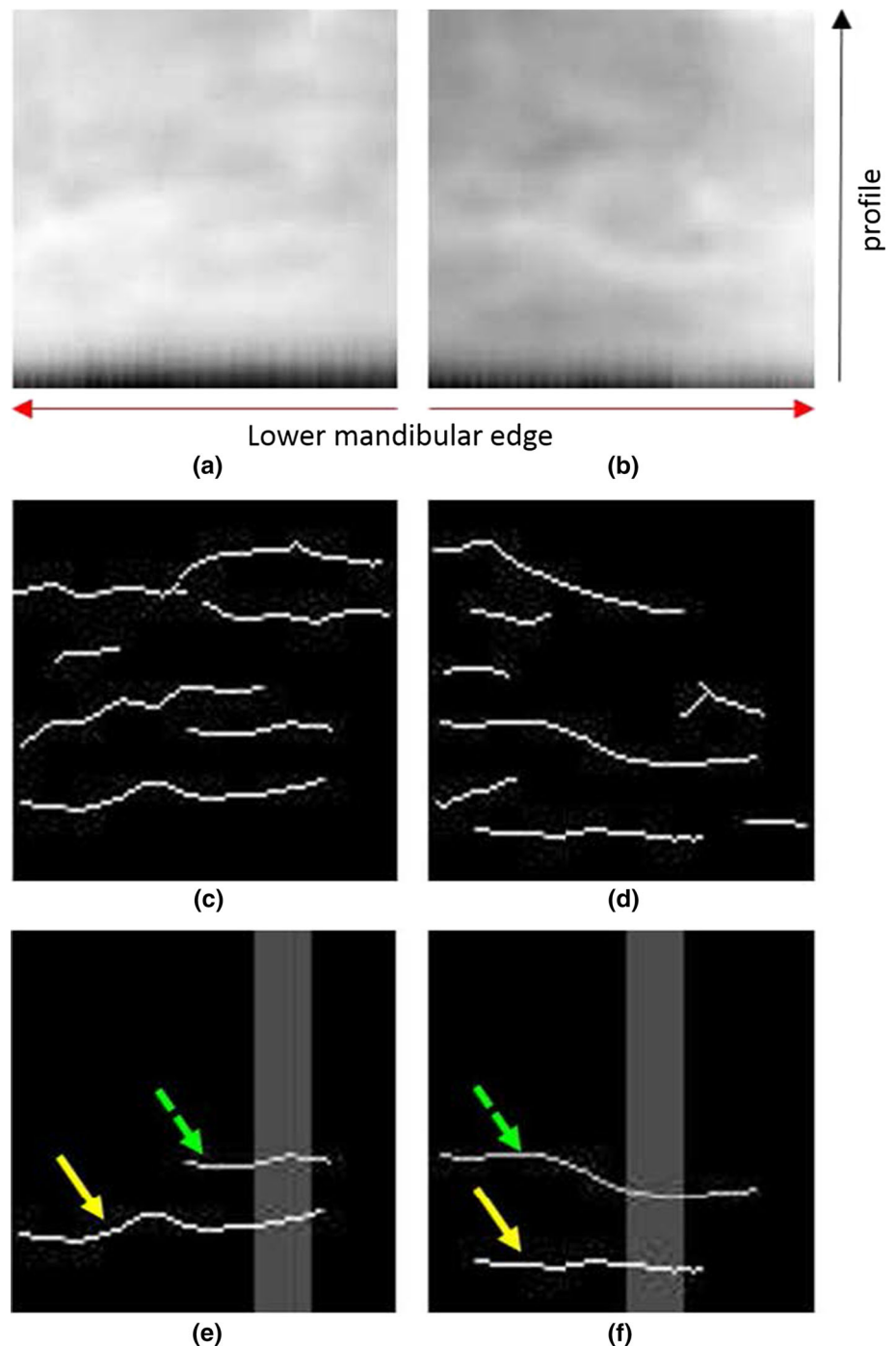
$$c_{i,j,\theta} = \frac{\vec{g}_{ij} \cdot \vec{p}_\theta}{|\vec{g}_{i,j}| \cdot |\vec{p}_\theta|} \tag{1}$$

where  $\vec{g}$  is the gradient vector and  $\vec{p}$  is the vector perpendicular to the presumed ridge,  $\Lambda_\theta$ . The output becomes one if the directions of these vectors are in concordance. The gradient vectors were determined in support regions,  $R_w$ , with a fixed length and a variable width above and below the presumed ridge. The convergence index at the point of interest was determined by

$$c(x) = \max_{R_w,\theta} \left( \frac{1}{n} \sum_{i,j} c_{i,j,\theta} \right) \tag{2}$$

where  $n$  is the number of pixels in  $R_w$ . For the MCW measurement, the length of  $R_w$  was set to 11 pixels and the width was varied from one to five pixels. Target ridges of −45 to 45 degrees with an increment of 15 degrees were considered. The point of interest was determined as a part of a ridge if the convergence index was above 0.5, which was set empirically; the output of a weak convergence below this threshold was set to zero. After line thinning, ridges less than 15 pixels were considered as “noise” and removed. The output image contained the ridges corresponding to the cortical peak and those corresponding to possible residues, as indicated by the lines in Fig. 4c, d.

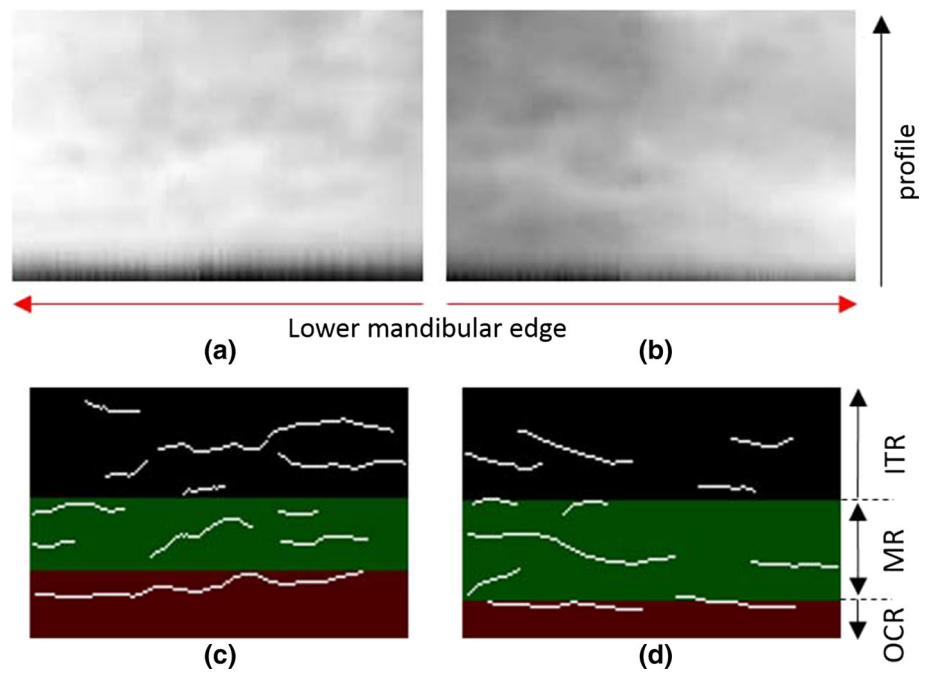
**Fig. 4** ROIs for the MCW measurement: **a, b** right and left ROIs, **c, d** output of the line convergence filter, and **e, f** selected cortex peak ridges (yellow arrows), potential ridges corresponding to cortical residue (green dotted arrows), and selected 15 profiles for the MCW measurement (gray areas)



In selecting a set of 15 profiles for MCW measurement, three rules were applied. First, the ridge corresponding to the densest part of the cortex (cortical peak) was present. The lowermost ridge in each ROI was considered as the cortical peak. Second, if the ridges corresponding to the cortical residues were present, the profiles were selected from these regions. In this study, any ridges detected within a vertical distance of 20 pixels from the cortical peak were determined as the residues. If no residues were present, all

regions meeting the first rule remained as candidates. Third, the average contrast in 15 consecutive profiles was greatest. Contrast is defined as the difference in pixel values of the cortical peak and the minimum pixel value between the peak and the residue, if it is present, or the pixel at a distance of 20 pixels from the peak, if no residue is present. The selected measurement region, corresponding to the consecutive 15 profiles, is presented as the gray area in Fig. 4e, f.

**Fig. 5** ROIs for feature analysis: **a, b** right and left ROIs and **c, d** output of line convergence filter and division into three regions of outer dense cortex region (OCR), marginal region (MR), and inner trabecular region (ITR)



The MCW measurement procedure from a profile has been described in detail elsewhere [13]. Briefly, the average downslope in the search range was determined as

$$G_{ave} = \left\{ \frac{\sum_{i=s}^e a_i - a_{i+1}}{n} \mid a_i > a_{i+1} \right\} \quad (3)$$

where  $s$  is the peak of the profile,  $e$  is the end of the search range,  $a_i$  is the corresponding pixel value (the profile amplitude), and  $n$  is the number of pixels satisfying  $a_i > a_{i+1}$ . If the cortical residue was present in the measurement region, the end of the search range was set at the residue ridge. Otherwise, the end was set as  $s + 19$  pixels. The pixel closest to the peak that met  $a_i - a_{i+1} \geq G_{ave}$  in the search range was determined as the upper cortical edge.

### ROI division and feature determination

The presence of horizontal ridges corresponding to the cortical residues is an important feature. The line convergence filter was also applied to the ROIs for feature analysis. For detecting smaller ridges, the length and maximum width of  $R_w$  were set to nine and three pixels, respectively. The other parameters were not changed. Figure 5c, d shows examples of the filter output.

To characterize cortical erosion, image features were determined in the cortical margin area. First, each ROI was separated into three regions: the outer “dense” cortex region (OCR), cortex margin region (MR), and inner trabecular bone region (ITR) as shown in Fig. 5c, d. The dense cortex region was defined as the rectangular region between the

lower mandible border, i.e., lower end of the ROI, and the horizontal line through the uppermost pixel of the cortical peak ridge. The upper border of the cortex margin region was determined using the profiles. Each profile, corresponding to a column of an ROI, was approximated by a third order polynomial function using a least squared fitting, and the inflection point  $I$  was determined by,

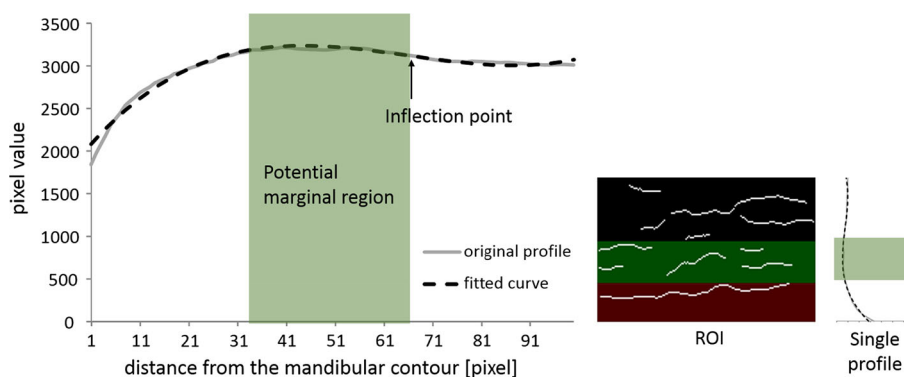
$$I = -\frac{b}{3a} \quad (4)$$

$$f(x) = ax^3 + bx^2 + cx + d \quad (5)$$

where  $a, b, c$  and  $d$  are the coefficients of the fitted curve (see Fig. 6). In Fig. 6, the potential marginal region based on this profile is indicated by the shaded area. The actual border between the margin and inner trabecular bone regions was set at the position of the average distance between the lower mandible border and the inflection points in 101 profiles. Figure 5c, d illustrates these regions.

The features included the area of MR (green area in Fig. 5c, d corresponding to potentially eroded region), number of the ridge pixels in MR (number of white pixels in Fig. 5c, d corresponding to potential residues), and ratio of the average pixel values of the ridge pixels in OCR and MR (means of original pixel values of white pixels in Fig. 5c, d). The textural features were determined based on eight GLCM corresponding to the four directions 0, 45, 90, and 135 degrees with a distance of five pixels in MR and the combined OCR and MR. For each matrix, 13 Haralick’s features were determined, yielding 104 features. The features included contrast, angular second moment, correlation, inverse difference

**Fig. 6** Polynomial curve fitting and determination of the inflection point for region division



moment, variance, difference entropy, difference variance, sum entropy, sum variance, entropy, sum average, information measure of correlation “1,” and information measure of correlation “2,” which are defined elsewhere [29].

### Feature reduction and MCD estimation

The total number of features including those described above and the MCW was 108, which was excessively large. Further, many of the textural features were expected to be highly correlated. To reduce the number of features, the criteria of individual utility and combinational redundancy were considered. First, the correlation between each feature and the subjective MCD was determined. The features with an absolute value of correlation less than 0.3 were removed from further consideration. For the remainder, PCA was applied to further reduce the feature dimension. Using the training dataset, the optimal number of principal components (PCs) was selected using a fivefold cross-validation test. The MCD was determined by SVR using the first  $n$  PCs. For evaluation of utilities of the image features alone and the combination of the image features and MCW, MCD was also estimated using the image features without MCW. The kernel function used was the radial basis function with gamma of 0.0625, and the cost and epsilon in loss function were 4.0 and 0.125, respectively, which were selected using the five-fold grid search. The parameters selected for MCD estimation without MCW were 0.0039, 16.0, and 0.016, respectively. The results were compared with the subjective MCD. The optimal  $n$  was determined based on the mean squared error. The test cases were projected to the PCA space spanned by the training cases, and the first  $n$  PCs were used for MCD estimation by the SVR model.

### Evaluation

The MCD estimation accuracy was evaluated by a comparison with the subjective MCD provided by the dental radiologist in terms of correlation. The estimated MCD was also compared with the BMD values. Classification perfor-

mances of the osteoporotic and normal cases and of high risk, i.e., osteoporosis and osteopenia, and low risk cases were evaluated by the receiver operating characteristic (ROC) analysis.

### Results

Using the training dataset, the utility of each feature was evaluated by correlation with the subjective MCD. The information measure of correlation “2” determined from the GLCM of zero degrees in the combined regions had the highest correlation of 0.789. Table 1 lists some of the features that are expected to be useful for MCD estimation. It can be observed that some of these features, including the MCW, have a high correlation value by themselves. With a threshold of 0.3, the number of features was reduced to 49. PCA was applied to these features, and the number of PCs used for MCD estimation using SVR was determined to be eight based on the minimum least squared error.

**Table 1** Correlation coefficient between the subjective MCD and each feature (top 10) for training dataset

Feature (region for GLCM, degree)	Correlation coefficient (absolute value)
Information measure of correlation 2 (CR, 0)	0.789
Information measure of correlation 1 (CR, 0)	0.766
Area of marginal region	0.750
MCW	0.730
Difference entropy (CR, 0)	0.699
Contrast (CR, 0)	0.682
Number of ridge pixels in marginal region	0.675
Difference variance (CR, 0)	0.672
Inverse difference moment (CR, 0)	0.659
Information measure of correlation 2 (CR, 135)	0.644

\*CR: combined outer and marginal cortical region

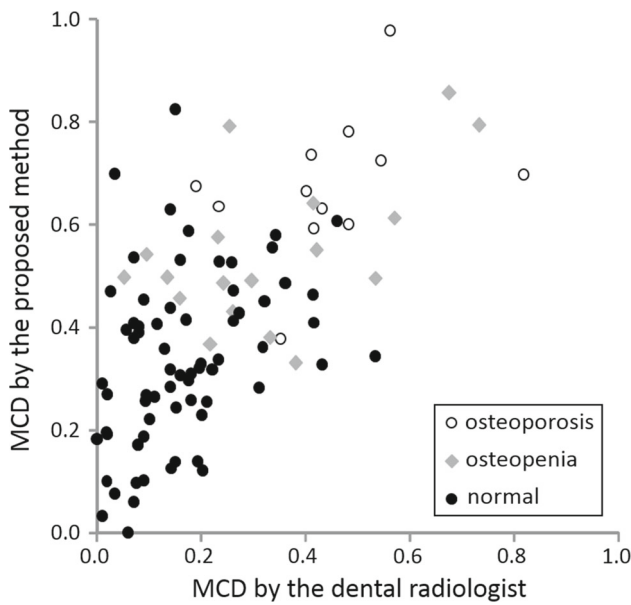


**Fig. 7** Relationship between MCDs determined by the dental radiologist and proposed method

The test cases were projected onto an 8-dimensional PC space spanned by the training dataset, and the MCDs were estimated using SVR. The relationship between the MCDs determined by the proposed method and the dental radiologist is shown in Fig. 7. Although MCD estimation was moderately successful, as indicated by the correlation coefficient of 0.617, there remains room for improvement compared with that for the training set of 0.841. When MCD was estimated using the image features without MCW, the correlation coefficient was 0.609. The correlation coefficient between the MCW alone and subjective MCD was  $-0.549$ . These results indicate the effectiveness of combining MCW and image features. Figure 8 a, b show the relationships between the BMD

and MCD by the dental radiologist and between the BMD and MCD by the proposed method, respectively. The correlation coefficient of  $-0.670$  is marginally higher than those between the subjective MCD and BMD ( $-0.600$ ), between the estimated MCD without MCW and BMD ( $-0.608$ ), and between the MCW alone and BMD (0.619). These results indicate the potential utility of the proposed MCD for osteoporotic risk assessment.

Figure 9a, b shows the ROC curves for the classification of the osteoporotic and non-osteoporotic cases and of the high-risk and low-risk cases, respectively. The areas under the curves (AUCs) for detecting osteoporotic cases using the MCD by the dental radiologist, the MCW alone, the MCD without MCW, and the MCD by the proposed method are 0.874, 0.830, 0.884, and 0.901, respectively. The AUCs for detecting the high-risk cases are 0.833, 0.835, 0.833, and 0.880, respectively. These are not statistically significantly different, although the difference between the MCW only and the MCD by the proposed method for detecting osteoporotic cases approached the statistical significant level ( $p = 0.06$ ). Note that for estimation of the MCD, the MCW measurement result was used as a feature. Our intention is not to replace the MCW by the MCD, rather to provide the MCD as additional information for assessing the risk of osteoporosis. Figure 10 shows a conceptual diagram of the system output. An MCW of 2.97 mm is at the borderline between suspected osteoporosis and normal. Inclusion of the high erosion degree suggests that the patient has a high risk of osteoporosis.

**Discussion**

We have previously proposed an automated method for measuring the MCW on DPRs for the early detection of

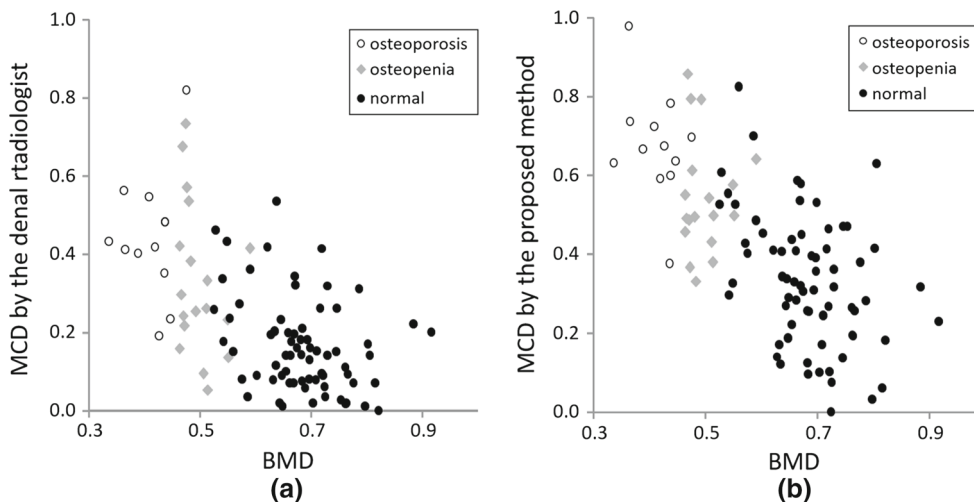


**Fig. 8** Relationships **a** between BMD and MCD by the dental radiologist and **b** between BMD and MCD by the proposed method

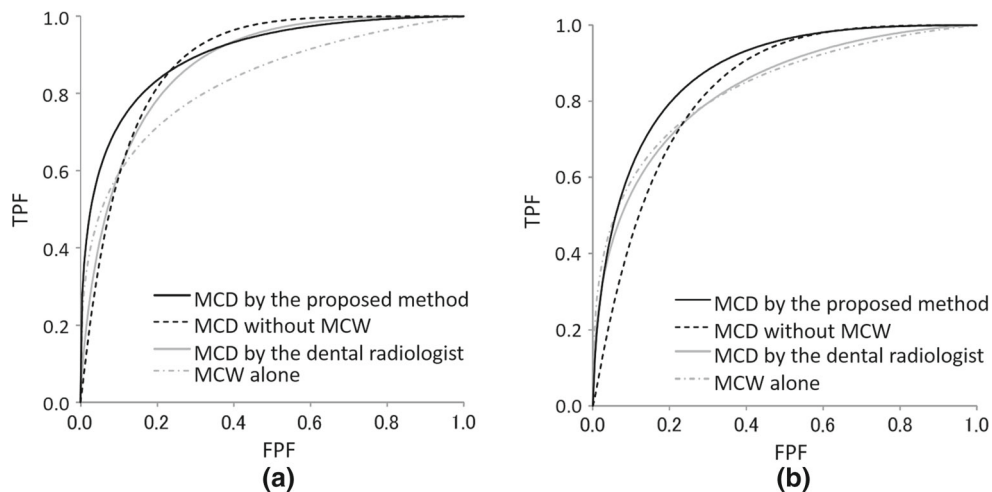
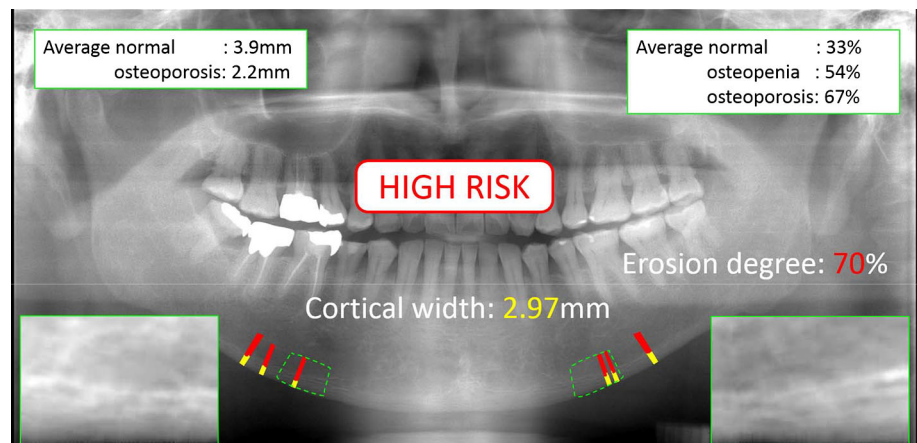


**Fig. 9** ROC curves for classification of **a** osteoporotic and non-osteoporotic cases and **b** high-risk and low-risk cases

**Fig. 10** Conceptual diagram of the system output showing the average MCW and estimated MCD with a high-risk alert



osteoporosis [13, 14]. The study demonstrated the potential usefulness of the computerized measurement using leave-one-out cross-validation with the training dataset. However, the osteoporotic change appears not only as a decrease in the MCW but also as porousness of the mandibular cortex. Characterization of the cortex may improve the sensitivity of osteoporosis detection and identification of individuals at a high risk. In our recent study, we attempted to classify the state of the mandibular cortex into three classes of MCI using four features [26]. Although the classification accuracies for the Class I and Class III cases were high with 94.6 and 94.1 %, respectively, the classification of Class II cases was difficult partially owing to the absence of a clear separation between the classes and a rather continual progressive change from Class I to III.

In this study, to overcome such difficulties and validate the utility with the independent cases, (1) the degree of cortex erosion was trained with and quantified as a continuous value instead of discrete classes and (2) the utility of the MCW and MCD for detecting high-risk cases were evaluated with an independent dataset with BMD data.

The cortex condition was graded in continuous degrees by a dental radiologist and used for the MCD estimation by an SVR. Having intermediate values as opposed to discrete classes could be useful in longitudinal comparison. It is expected that the training can be performed more effectively because the textural change in the cortex is gradual. To support this, SVM was trained with the categorized data rather than the continuous MCD. The outputs were the classification category and the likelihood for each class. Using the output likelihood of Class I (normal), the AUC for detecting the high-risk group was 0.874 (vs. 0.880 for MCD;  $p > 0.05$ ). The AUCs for detecting the osteoporotic group using the likelihood of Class I and Class III (osteoporotic) were 0.859 (vs. 0.901 for MCD;  $p > 0.05$ ) and 0.777 ( $p = 0.02$ ), respectively. Therefore, the performance was slightly improved using the continuous data, although the differences were not statistically significant using the Class I likelihood data.

DPR imaging conditions are not standardized. Therefore, the image quality varies considerably depending on the dental clinics and imaging equipment. Hence, it is preferable that

the computerized system is robust to images with different quality. In this study, we evaluated the proposed method with a new database obtained using a different imaging system. The correlation between the subjective and estimated MCDs for the test dataset was not very high compared with that for the training dataset; however, the moderate correlation with the BMD and comparable AUCs to those for the MCD by the dental radiologist indicate the potential usefulness of the estimated MCD for the risk assessment.

This study has limitations. Although the proposed method was evaluated with an independent database, these images were obtained at the university hospital and do not include images with the variety of image quality expected from community dental clinics. We are investigating a preprocessing method to standardize DPRs. The proposed method must be evaluated with a large and heterogeneous dataset with and without such preprocessing techniques.

The gold standard for osteoporosis and osteopenia in this study was based on the BMD at the distal forearm. These BMD values may not be related to severe osteoporotic fractures in the spine and hip. We assumed that all patients have no non-traumatic fractures on the basis of self-reporting. The presence of no asymptomatic fractures is unknown because these patients visited the periodontal department for dental examination and spine radiographs were not obtained. The definitive diagnosis should be determined by presence of fractures. Our goal in this study is to inform patients with high risk and suggest them to receive detailed examinations or a standard osteoporosis screening. For that purpose, BMD measurement at forearm performed with a simple equipment was employed as the gold standard in this study. However, the proposed method should be tested with cases having the BMD measured at the spine and hip bone and the status of fractures.

In recent cross-sectional study, Zebaze et al. [32] compared cortical and trabecular bone mass using CT of distal forearm and measured cortical porosity using scanning electron microscopy of femur specimens. They suggested that the most bone loss occurring at older ages is cortical and the measurement of cortical porosity could improve identification of individuals at risk of fractures. Therefore, our proposed method of quantifying cortical erosion may have potential in identifying those at high and low risk of fractures.

It is known that the prevalence of osteoporosis is different for men and women. The texture and characteristics of mandibular bone might be different, and MCD could be estimated better using separate models for men and women. However, the training dataset includes one osteoporotic case of man and the test dataset includes three osteopenic and one osteoporotic cases of men, which makes the reliable analysis difficult. The separate analysis will be considered when we obtained a sufficient number of data in the future.

## Conclusion

We investigated an automated scheme for supplemental risk assessment of osteoporosis using DPRs. The experimental results show the effectiveness of the proposed cortex feature analysis for quantification of cortex erosion. Use of continuous degree can facilitate perceiving a gradual change in the cortex and therefore more effectively assess the progression. The MCD can supplement the MCW in detecting osteoporotic and osteopenic patients. The computerized quantification of the MCW and MCD on DPRs has a potential utility for osteoporotic risk assessment through dental examination with no extra cost.

**Acknowledgments** Authors appreciate the members of the Fujita Laboratory at Gifu University and dental CAD research group at Asahi University School of Dentistry, Aichi Gakuin University and Media, Co., Ltd. for their valuable discussion.

## Compliance with ethical standards

**Funding** This study was supported in part by Grant-in-Aid for Scientific Research (b) JSPS KAKENHI Grant Number 26293402 and Grant-in-Aid for Scientific Research on Innovative Areas (Multidisciplinary Computational Anatomy), MEXT, Japan, Grant Number 26108005.

**Conflict of interest** The authors declare that they have no conflict of interest.

## References

1. Kanis JA on behalf of the World Health Organization Scientific Group (2007) Assessment of osteoporosis at the primary health-care level. WHO Technical Report. University of Sheffield, UK
2. Cummings SR, Melton LJ III (2002) Epidemiology and outcomes of osteoporotic fractures. *Lancet* 359:1761–1767
3. Johnell O, Kanis JA (2006) An estimated of the worldwide prevalence and disability associated with osteoporotic fractures. *Osteoporos Int* 17:1726–1733
4. Bollen AM, Taguchi A, Hujoel PP, Hollender LG (2000) Case-control study on self-reported osteoporotic fractures and mandibular cortical bone. *Oral Surg Oral Med Oral Pathol Oral Radiol Endod* 90:518–524
5. Devlin H, Horner K (2002) Mandibular radiomorphometric indices in the diagnosis of reduced skeletal bone mineral density. *Osteoporos Int* 13:373–378
6. Taguchi A (2010) Triage screening for osteoporosis in dental clinics using panoramic radiographs. *Oral Dis* 16:316–327
7. American Dental Association Survey Center (2007) 2000 survey of dental practice: characteristics of dentists in private practice and their patients. American Dental Association, Chicago
8. Shimano T, Suzuki Y, Sasaki T (2002) Long-term trend of dental radiographic examination in Japan—analysis on health insurance data. *Dent Radiol* 42:9–21 (in Japanese)
9. Arifin AZ, Asano A, Taguchi A, Nakamoto T, Ohtsuka M, Tsuda M, Kudo Y, Tanimoto K (2006) Computer-aided system for measuring the mandibular cortical width on dental panoramic radiographs in identifying postmenopausal women with low bone mineral density. *Osteoporos Int* 17:753–759

10. Kavitha MS, Asano A, Taguchi A, Heo MS (2013) The combination of a histogram-based clustering algorithm and support vector machine for the diagnosis of osteoporosis. *Imaging Sci Dent* 43:153–161
11. Allen PD, Graham J, Farnell DJJ, Harrison EJ, Jacobs R, Nicopolou-Karayianni K, Lindh C, van der Stelt PF, Horne K, Devlin H (2007) Detecting reduced bone mineral density from dental radiographs using statistical shape models. *IEEE Trans Inform Technol Biomed* 11:601–610
12. Roberts MG, Graham J, Devlin H (2010) Improving the detection of osteoporosis from dental radiographs using active appearance models. *IEEE Int Symposium Biomed Imaging Nano Macro* 2010:440–443
13. Muramatsu C, Matsumoto T, Hayashi T, Hara T, Katsumata A, Zhou X, Iida Y, Matsuoka M, Wakisaka T, Fujita H (2013) Automated measurement of mandibular cortical width on dental panoramic radiographs. *Int J Comput Assist Radiol Surg* 8:877–885
14. Horiba K, Muramatsu C, Hayashi T, Fukui T, Hara T, Katsumata A, Fujita H (2014) Automated measurement of mandibular cortical width on dental panoramic radiographs for early detection of osteoporosis: extraction of linear structures. *Med Imag Tech* 32:342–346 (in Japanese)
15. Taguchi A, Asano A, Ohtsuka M, Nakamoto T, Suei Y, Tsuda M, Kudo Y, Inagaki K, Noguchi T, Tanimoto K, Jacobs R, Klemetti E, White SC, Horner K (2008) Observer performance in diagnosing osteoporosis by dental panoramic radiographs; results from the osteoporosis screening project in dentistry (OSPD). *Bone* 43:209–213
16. Klemetti E, Kolmacov S, Kroger H (1994) Pantomography in assessment of the osteoporosis risk group. *Scand J Dent Res* 102:68–72
17. Law AN, Bollen AM, Chen SK (1996) Detecting osteoporosis using dental radiographs: a comparison of four methods. *JADA* 127:1734–1742
18. Shrout MK, Hildebolt CF, Potter BJ, Brunsten TKB, Pilgrm TK, Dotson M, Yokoyama-Crothers M, Hauser J, Cohen S, Kardaris E, Civitelli R, Hanes P (2000) Comparison of morphological measurements extracted from digitized dental radiographs with lumbar and femoral bone mineral density measurements in postmenopausal women. *J Periodontol* 71:335–340
19. Southard TE, Southard KA, Lee A (2001) Alveolar process fractal dimensional and postcranial bone density. *Oral Surg Oral Med Oral Pathol Oral Radiol Endod* 91:486–491
20. Bollen AM, Taguchi A, Hujoel PP, Hollender LG (2001) Fractal dimension on dental radiographs. *Dentomaxillofacial Radiol* 30:270–275
21. Tosoni GM, Lurie AG, Cowan AE, Burleson JA (2006) Pixel intensity and fractal analyses: detecting osteoporosis in perimenopausal and postmenopausal women by using digital panoramic images. *Oral Surg Oral Med Oral Pathol Oral Radiol Endod* 102:235–241
22. Nakamoto T, Taguchi A, Ohtsuka M, Suei Y, Fujita M, Tsuda M, Sanada M, Kudo Y (2008) A computer-aided diagnosis system to screen for osteoporosis using dental panoramic radiographs. *Dentomaxillofacial Radiol* 37:274–281
23. Nakamoto T, Mahmud Uz Z, Taguchi A, Tanimoto K (2014) New advanced computer-aided diagnosis system to screen osteoporosis using dental panoramic radiographs. *Proc Int J CARS* 9:360–361
24. Roberts M, Graham J, Devlin H (2013) Image texture in dental panoramic radiographs as a potential biomarker of osteoporosis. *IEEE Trans Biomed Eng* 60:2384–2392
25. Kavitha MS, An SY, An CH, Huh KH, Yi WJ, Heo MS, Lee SS, Choi SC (2015) Texture analysis of mandibular cortical bone on digital dental panoramic radiographs for the diagnosis of osteoporosis in Korean women. *Oral Surg Oral Med Oral Pathol Oral Radiol* 119:346–356
26. Horiba K, Muramatsu C, Hayashi T, Fukui T, Hara T, Katsumata A, Fujita H (2015) Automated classification of mandibular cortical bone on dental panoramic radiographs for early detection of osteoporosis. *Proc SPIE Med Imaging 2015: Comput-Aided Diagnosis* 9414:94132J1–94132J6
27. Kirsch RA (1971) Computer determination of the constituent structure of biological images. *Comput Biomed Res* 4:1315–1328
28. Kobatake H, Hashimoto S (1999) Convergence index filter for vector fields. *IEEE Trans Image Process* 8:1029–1038
29. Haralick RM, Shanmugam K, Dinstein I (1973) Textural features for image classification. *IEEE Trans Sys Man Cyber* 3:610–621
30. Chang CC, Lin CJ (2011) LIBSVM: a library for support vector machines. *ACM Trans Intell Syst Technol* 27-1-27. Software available at <http://www.csie.ntu.edu.tw/~cjlin/libsvm>
31. Benson BW, Prihoda TJ, Glass BJ (1991) Variations in adult cortical bone mass as measured by a panoramic mandibular index. *Oral Surg Oral Med Oral Pathol* 71:349–356
32. Zebaze RMD, Ghasem-Zadeh A, Bohte A, Iuliano-Burns S, Mirams M, Price RI, Mackie EJ, Seeman (2010) Intracortical remodeling and porosity in the distal radius and post-mortem femurs of women; a cross-sectional study. *Lancet* 375:1729–1736